


Directed negative-weight percolationC. Norrenbrock,^{*} M. M. Mkrtchian,[†] and A. K. Hartmann[‡]
Institut für Physik, Universität Oldenburg, 26111 Oldenburg, Germany (Received 20 February 2019; revised manuscript received 19 July 2019; published 12 August 2019)

We consider the negative-weight percolation model on *directed* graphs. In particular, we study the model on a two-dimensional, weighted, periodic, centered square lattice. Bond weights are taken from a distribution that allows for both positive and negative values. For a given realization of the disorder, a minimally weighted directed loop and path configuration is determined by performing a nontrivial transformation of the original lattice into a minimum-weight perfect matching problem. For this problem, fast polynomial-time algorithms are available, thus we could study large systems with high accuracy. Depending on the fraction of negatively and positively weighted bonds on the lattice, a continuous phase transition is identified and its characterizing critical exponents are estimated by means of a finite-size scaling analysis. We observe a strong change of the universality class with respect to standard directed percolation as well as with respect to undirected negative-weight percolation. Furthermore, the relation to directed polymers in random media is illustrated.

DOI: [10.1103/PhysRevE.100.022113](https://doi.org/10.1103/PhysRevE.100.022113)**I. INTRODUCTION**

The study of phase transitions is one of the main areas in statistical physics [1]. In particular one is interested in universal properties, which are independent of microscopic details, but depend on symmetry properties of the underlying model only. This allows one, for second-order phase transitions, to group systems or models in universality classes, which are characterized by a set of critical exponents and their functional relations, i.e., scaling laws. One of the most basic and intensively studied universality classes is that of standard percolation [2,3], where a certain fraction p of sites or bonds is occupied. Thus, one addresses the basic question of connectivity, such that within numerical studies, one has to obtain connected clusters of occupied sites. Beyond a critical value p_c , the percolation threshold, a system-spanning cluster emerges. Beyond its fundamental importance, often other phase transitions can be understood, after a suitable transformation, in terms of percolation, e.g., the percolation of Fortuin-Kasteleyn clusters [4] in the Ising model.

In standard percolation, bonds do not carry any weight, thus, one can assume all weights being one, i.e., they are positive. Recently, a bond percolation model called “negative-weight percolation” (NWP) was introduced [5], where random weights are attached to bonds, and, in particular, weights of either sign are allowed. For NWP, one is interested in a collection of loops and possibly paths which exploit the negative bonds as much as possible, such that the global weight is minimized. As an interpretation of the NWP problem, one can imagine an agent that takes a trip on a graph along the path. Whenever he travels along a positively weighted bond, the agent has to pay some resource according to the positive

value. However, he will harvest some resource, if he travels along a negatively weighted bond. Therefore, the optimal loop and path configuration obtained in the context of the NWP problem provides the optimal route of the agent (path), possibly in competition with other agents (loops), to gain as many resources as possible. Only paths or loops which lead to a larger amount of harvested resources as compared to the paid resources will occur. Algorithmically, this means special global optimization polynomial-time “matching” algorithms have to be applied, see Sec. II. This is in contrast to standard percolation, where the clusters can be constructed by a local algorithm. Note that the algorithm in its basic implementation yields a collection of loops globally minimizing the weight. But by suitably “decorating” the lattice, also the creation of one or several paths can be enforced, which is useful to study percolation phenomena.

It has been shown that for standard NWP two distinct phases can be identified depending on a disorder parameter ρ , which controls the amount of negative weights: (i) for small ρ all geometric objects are rather small and straight-lined, which reflects a self-affine scaling; (ii) for large ρ the geometric objects scale self-similar and can wind around the lattice, i.e., percolate. In Ref. [5] the disorder-driven phase transition is investigated by means of finite-size scaling analyses and it turns out that the critical exponents are universal in 2D (different lattice geometries and disorder distribution are studied). The NWP model exhibits a new type of behavior giving rise to a different universality class compared to standard percolation, maybe not unexpectedly due to the global nature of the model. Further studies regarding isotropic NWP address the influence of dilution on the critical properties [6], the upper critical dimension ($d_u = 6$) [7], another upper critical dimension ($d_u^{\text{DPL}} = 3$) for densely packed loops far above the critical point [8], the mean-field behavior on a random graph with fixed connectivity [9], Schramm-Loewner evolution properties of paths on 2D lattices [10], and loop-length distributions in several dimensions [11].

^{*}christoph.norrenbrock@uni-oldenburg.de[†]mitchell.mger.mkrтчian@uni-oldenburg.de[‡]alexander.hartmann@uni-oldenburg.de

In standard percolation, there is no directional information in the connectivity pattern. Thus, not surprisingly, the critical exponents describing this phase transition differ from those that describe the phase transition in directed percolation (DP) [12], which is a variant of standard percolation, where bonds carry a direction leading to an anisotropic behavior. Note that this directionality can be interpreted as time direction, making DP relevant for the description of nonequilibrium processes. Because of the anisotropic nature of the cluster building process in DP, correlations are not governed by one but two correlation lengths: ξ_{\parallel} and ξ_{\perp} . In DP the percolation threshold separates one phase ($p < p_c$), where all cluster building processes stop eventually, so just finite clusters can occur, from another phase ($p > p_c$), in which clusters can survive each time step and, as a consequence, can grow infinitely large.

So far the above mention NWP model has been investigated only on nondirected lattices or graphs. Thus, as compared to the change which occurs when moving from standard to directed percolation, it is valid to ask whether the directed variant of NWP, which is introduced and studied in this work, gives again rise to a new type of behavior.

While DP is defined as a local growth process, the path-like clusters in NWP emerge due to global optimization. This is also true for directed polymers in random media (DPRM) [13], but unlike NWP, DPRM does not feature a phase transition, since all paths are system spanning by construction. In directed NWP, as we will see below, the paths may differ in length. Also the appearance of negatively weighted loops that cannot be crossed by the path influence its shape, since the loops block regions of the underlying lattice, which become inaccessible to the path. Furthermore, in directed NWP (in contrast to DPRM) the path can span the system several times, allows it to pick up many negative weights. As a consequence, it can be affected by itself. For those reasons the path in directed NWP cannot be considered as optimal on its own and its scaling behavior might differ from DPRM. Nevertheless, it will be outlined in this article that NWP and DPRM are partially related to each other.

In this article we study by computer simulations [14] the disorder-driven, geometric phase transition at ρ_c and determine its characterizing critical exponents. The remainder of this article is organized as follows. In Sec. II, we introduce the model in more detail and explain the algorithm. In Sec. III, we describe the finite-size scaling technique that has been used to estimate the critical exponents numerically and present our results. We close with a summary in Sec. IV.

II. MODEL AND ALGORITHM

The underlying graph $G = (V, E)$, V denoting the set of nodes and E the set of bonds (often called edges in graph theory), at hand is a two-dimensional, directed square lattice. For our geometry, the bonds (i, j) point either to the bottom left or bottom right [cf. Fig. 2(a)]. The lattice boundaries are periodic meaning the lattice can be considered as placed on a torus in a topological sense. Each bond $e \in E$ carries a weight ω_e that is taken, like in previous studies [5–7] (but somehow arbitrary, due to universality), from a “Gauss-like” distribution

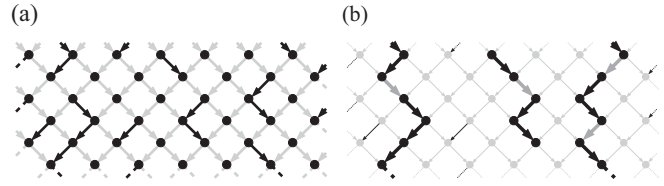


FIG. 1. (a) A realization of the disorder on a 7×6 lattice. The weight of the bonds is -1 (black) or $+1$ (gray). (b) The corresponding solution of the directed NWP problem (thick), exhibiting one path and two loops.

characterized by a tunable disorder parameter ρ :

$$P(\omega) = (1 - \rho)\delta(\omega - 1) + \rho \exp(-\omega^2)/\sqrt{2\pi}, \quad 0 \leq \rho \leq 1. \quad (1)$$

Thus, the proportion of negative and positive weights can be tuned by a disorder parameter ρ . The shape of the lattice is rectangular in all simulations, with different side lengths L_{\parallel} and L_{\perp} , so the number of nodes is $N = |V| = L_{\parallel} \cdot L_{\perp}$. Due to the construction of the underlying periodic lattice, L_{\parallel} has to be even, and L_{\perp} has to be odd. Bond directions are arranged as can be seen in Fig. 2(a). According to this illustration, L_{\parallel} describes the number of rows and $2L_{\perp}$ the number of columns of the lattice.

Given a realization of the disorder, an optimal configuration consisting of an arbitrary number of loops, i.e., closed paths, and one additional path (possibly with zero length) is computed. Mathematically, paths and loops are subsets of bonds. Here we chose to study the model in the way such that each configuration must fulfill following requirements: (i) One endpoint of the path is pinned at the top middle. However, it is also allowed that no path occurs. (ii) The loops and the path are not allowed to cross or even touch each other. (iii) The configurational energy,

$$\mathcal{E} = \sum_{\mathcal{L} \in \mathcal{C}} \omega_{\mathcal{L}}, \quad (2)$$

has to be minimized. Here $\omega_{\mathcal{L}}$ denotes the sum $\sum_{e \in \mathcal{L}} \omega_e$ of all bond weights belonging to loop or path \mathcal{L} . Note that Eq. (1) provides real numbers, so the optimal configuration is unique for each realization of the disorder. Since the number of loops is not specified and even the path might not appear (zero length), also an empty configuration might be valid. This would be the case, e.g., if all bonds carried a positive weight. Loops and also the path can solely appear, if their weight is negative, otherwise \mathcal{E} would not be minimal, since an empty configuration has $\mathcal{E} = 0$. Furthermore, since all bonds point either to the left or right bottom, loops can appear only, if they span the lattice in vertical direction. Therefore, their smallest length is L_{\parallel} . Figure 1(a) shows a realization of the disorder on a 7×6 lattice, in which the weight of the black bonds is -1 and of the gray ones $+1$. The corresponding optimal configuration (represented by thick bonds) is illustrated in Fig. 1(b). It consists of two loops and one path and its configurational energy is $\mathcal{E} = -8$.

To find the optimal configuration, common shortest path algorithms cannot be used, since they are not able to handle negatively weighted bonds in a proper way. Note that it is

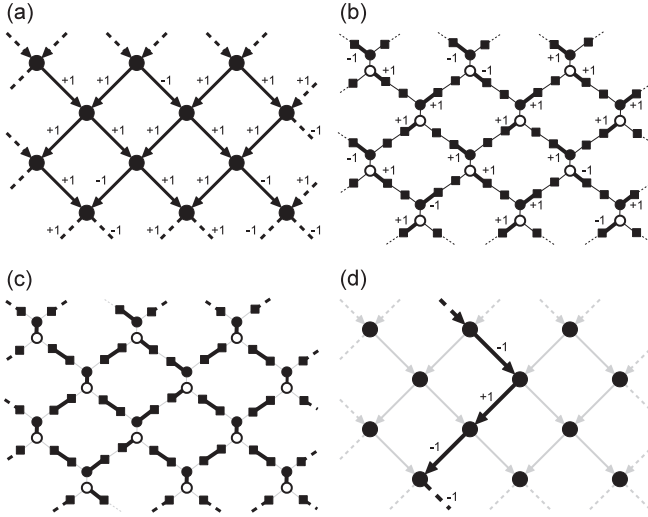


FIG. 2. Illustration of the algorithmic procedure for a periodic lattice of size $L_{\parallel} = 3$ and $L_{\perp} = 4$. For the sake of clarity, the procedure is just depicted for a directed lattice that does not contain a finite path. In Sec. II it is described how the construction of the auxiliary graph must be altered to force a path in the lattice that starts at the top middle and terminates at any node. (a) Original lattice with weighted, directed bonds. (b) Auxiliary graph with proper weight assignment. The thick bonds carry the weight as the respective bonds in the original graph. The weights of all other bonds are zero. (c) Illustration of the MWPM: black bonds are matched and gray ones are unmatched. For the sake of clarity, bond weights are not depicted. (d) Reconstruction to the original lattice taking the MWPM result into account.

tempting to think that one could shift all weights to positive values by adding a constant to all weights, but this actually changes the behavior, as it was detailed before [5]. To obtain the minimum-energy configuration, we transform the original graph to an appropriate auxiliary graph. The basic approach how to set up these auxiliary graphs to calculate shortest paths in graphs involving negative weight is established in computer science [15]. Nevertheless, since this auxiliary graph is different from the undirected NWP case, and for the convenience of the reader, we present the transformation in detail in the following. The main step is, having the auxiliary graph, to determine a *minimum-weight perfect matching* (MWPM) [16–18]. The MWPM provides all information to reconstruct the original graph exhibiting the correct loop and path configuration. Figure 2 is an illustration of the algorithmic procedure for a given realization of the disorder for a periodic lattice of size $L_{\parallel} = 3$ and $L_{\perp} = 4$. For reasons of clarity, only loops but no path can occur here. Furthermore, for simplicity only bond weights $+1$ and -1 are used in the example in contrast to Eq. (1). Guided by Fig. 2, we give a concise description how the algorithm works. Afterwards, we explain how the algorithm must be altered to enable the appearance of a path.

(1) The transformation to the auxiliary graph $G' = (V', E')$ is illustrated in Fig. 3 for two nodes. All labels in the figure will be used in the following description. First, all nodes $u \in V$ are duplicated to u_1 and u_2 , i.e., $u_1, u_2 \in V'$. These duplicated nodes are connected in G' by a new undirected

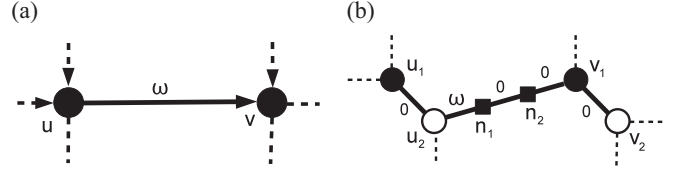


FIG. 3. The mapping procedure to the auxiliary graph shown for two nodes of the original graph.

bond $\{u_1, u_2\}$ with weight zero. Subsequently, for all bonds $(u, v) \in E$ (directed from u to v) two additional nodes n_1, n_2 and three bonds $\{u_2, n_1\}$, $\{n_1, n_2\}$, and $\{n_2, v_1\}$ are added to G' , forming a path connecting u_2 to v_1 via n_1 and n_2 . The weight ω of bond (u_2, v_1) is assigned either to $\{u_2, n_1\}$ or $\{n_2, v_1\}$ (the choice does not change the final result). The other two bonds get a weight of zero. The resulting auxiliary graph is shown in Fig. 3 for two nodes and in Fig. 2(b) for a 3×4 lattice.

(2) A MWPM is determined on the auxiliary graph via exact combinatorial optimization algorithms [19]. A *matching* M of a graph is a subset of bonds $M \subset E$, such that no two edges are incident to the same node, i.e., no edges “touch.” The nodes connected by a bond in M are called *matched*. A *perfect matching* is a matching of cardinality $N/2$, i.e., each node is connected in M to another node. Finally, the weight of a matching is the sum of the weights of the bonds in the matching. Thus, a minimum (perfect) matching is the minimum-one among all (perfect) matchings. It is possible in polynomial time to obtain a MWPM. The algorithm we use exhibits a worst-case complexity $O(N^3)$. For the given example, the MWPM is illustrated in Fig. 2. Bonds that belong to the MWPM are represented bold and black.

(3) After determining the MWPM, the original graph can be reconstructed. We will now explain how this works, and this will explain why the auxiliary graph is constructed as it is. We consider a bond that links two additional nodes (in Fig. 3 these nodes are n_1 and n_2). There are two cases: either $\{n_1, n_2\}$ does not belong to the MWPM, or it does. In the first case, since the matching is perfect, n_1 must be matched to u_2 and n_2 must be matched to v_1 since for both nodes no other possible matching partners are available. Thus, through these two edges in the MWPM, the weight ω appears in the MWPM’s weight. In fact, this pair $\{u_2, n_1\}$ and $\{n_2, v_1\}$ of matched bonds with weight ω corresponds to the bond (u, v) (with weight ω) to be part of the path. The path has, in general, to continue; i.e., it must lead into u and go out of v . That this will happen automatically becomes clear from the following observation: Since u_2 is already matched, the bond $\{u_2, u_1\}$ will not be part of the MWPM. Therefore, u_1 in turn has to be matched to one of its other neighbors, which are nodes of “ n -type,” say n'_2 . Thus, through the definition of a matching, n'_2 cannot be matched to n'_1 , hence, n'_1 must be matched to one node of “ 2 -type,” call it w_2 . Hence, one has again a pair $\{w_2, n'_1\}$ and $\{n'_2, u_1\}$ of bonds, which corresponds to the original edge (w, u) of G and is part of the path. Thus, the fact that the path leaves node u via (u, v) forces with the properties of a MWPM that the path must enter node u by some edge (w, u) . In the same way, the path must leave v . This is exactly the defining property of an ongoing path.

In the second case, when $\{n_1, n_2\}$ belongs to the MWPM, it will add zero weight. Furthermore, the bonds $\{u_2, n_1\}$ and $\{n_2, v_1\}$ cannot be part of the MWPM, since each node is matched to exactly one other node. Therefore, the bond (u, v) will not be part of a path. Furthermore, this means for u_2 (and similarly for v_1) that it can be either matched to another n -type node (which means that a path leaves u through another bond) or that it is matched to u_2 (no path runs through u at all). In particular, the MWPM could contain only bonds of type $\{n_1, n_2\}$ and of type $\{u_1, u_2\}$. This has total weight zero and corresponds to no paths at all.

Principally, the auxiliary graph can be altered to allow the loops and path to intersect each other. For this purpose the original nodes have to be quadrupled and further additional bonds have to be added. It has been shown in Ref. [5] in regard to undirected lattices that such an alteration does not change the universality class. Therefore, this modification has not been considered by us.

As the algorithm has been presented, due to the property that all nodes have to be matched to another node in the auxiliary graph, each node in the original graph will be incident to zero or two bonds belonging to a path. Thus, only closed paths, i.e., loops can appear so far. To enable a path, the auxiliary graph must be expanded. After constructing the auxiliary graph as described above, the white duplicate of the original node in the top middle gets connected to the black duplicates of all other original nodes with a bond carrying zero weight. This means technically the path is also a loop, but the “returning” part of the loop is “hidden” with respect to the original lattice, such that it appears as a path. Therefore, for the current auxiliary lattice, exactly one path is possible, which starts in the top middle node and may end in any other node (returning hiddenly). Such an auxiliary graph is not planar and contains many additional bonds, therefore, we do not depict this additional specification in the illustration Fig. 2. Note finally that due to the global nature of the optimization problem, it is not possible to restrict the number of loops. Thus, the path we are interested in here, may always occur together with some loops. But in the percolation transition region they are usually well separated, so we assume that they do not influence each other much. This is also supported by our comparison with some scaling behavior of DPRM, which is always only one path.

III. RESULTS

The NWP model exhibits a geometrical continuous phase transition. For a small amount of negative weights, the path would appear rather short and loops would not appear at all, if the system size were chosen sufficiently large. This can be seen in Fig. 4, where optimal configurations for different values of ρ on a lattice of size $L_{\parallel} = 32$ and $L_{\perp} = 33$ are shown. For small values of ρ , the path is rather short because otherwise its total weight cannot be minimum, and the formation of loops is suppressed, because each possible loop has length $O(L_{\parallel})$ and thus would also collect too many positively weighted bonds. This is clearly different in the undirected variant of the model, where also small loops will appear, even if ρ is small [5]. However, if ρ is large, then the path might grow very long and even multiple loops will occur. The two

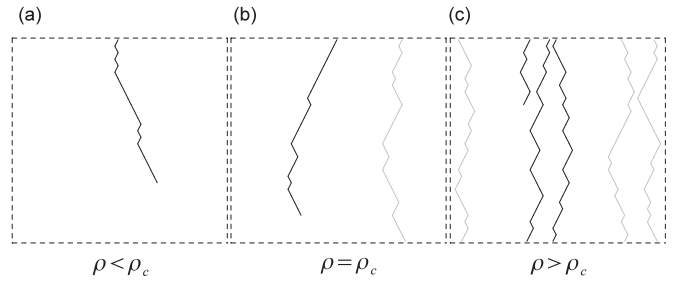


FIG. 4. Illustration of minimum-weight configurations consisting of loops (gray) and one path (black) in a directed, two-dimensional, centered square lattice of side length $L_{\parallel} = 32$ and $L_{\perp} = 33$ with periodic boundary conditions. The path is forced to start at the top middle of the lattice. For small values of ρ , there does not appear a loop and also the path does not span the lattice. At $\rho = \rho_c$ one percolating loop occurs. For large values of ρ , there are many spanning loops and also the path percolates.

regions, in which lattice-spanning, i.e., percolating, loops or paths will or, respectively, will not occur, are separated by a certain value of $\rho = \rho_c$, the critical point. In the thermodynamic limit there are no lattice-spanning objects in the lattice for $\rho < \rho_c$, and one or several ones for $\rho > \rho_c$.

In this section we determine the critical point and estimate the critical exponents that characterize the phase transition by means of a finite-size scaling analysis. A common scaling assumption [3] that is typically used for undirected models cannot be applied here. Due to the anisotropic nature of the underlying lattice, there are two different correlation lengths that have a different asymptotic behavior,

$$\xi_{\parallel} \sim |\rho - \rho_c|^{-\nu_{\parallel}}, \quad \xi_{\perp} \sim |\rho - \rho_c|^{-\nu_{\perp}}, \quad (3)$$

in the thermodynamic limit, with ν_{\parallel} and ν_{\perp} being the critical exponents describing the power-law divergence of the correlation lengths. For investigating finite-size scaling in systems with anisotropic critical behavior it is required to fix the generalized aspect ratio $L_{\parallel}/L_{\perp}^{\theta}$ with anisotropy exponent $\theta = \nu_{\parallel}/\nu_{\perp}$ [20,21]. To find out the proper value of θ , we consider $\xi_{\perp} \sim \xi_{\parallel}^{1/\theta}$. For $L_{\perp} \rightarrow \infty$ and finite L_{\parallel} the correlation length ξ_{\parallel} is limited by L_{\parallel} when approaching the critical point [20], resulting in

$$\xi_{\perp}(L_{\parallel}, L_{\perp} \rightarrow \infty) \sim L_{\parallel}^{1/\theta}. \quad (4)$$

Therefore, we take $\xi_{\perp}(L_{\parallel}, L_{\perp} \rightarrow \infty)$ as the lateral extension of the path. This means that for each value of L_{\parallel} we vary L_{\perp} and extrapolate the value of ξ_{\perp} for $L_{\perp} \rightarrow \infty$ [main plot of Fig. 5(b)]. Then we can determine $\theta = 1.59(2)$ according to Eq. (4), see inset of Fig. 5(b).

The main simulations were performed for fixed generalized aspect ratio $L_{\parallel}/L_{\perp}^{\theta}$. It is expected [21] that cluster-related quantities $y(\rho, L_{\parallel}, L_{\perp})$ can be rescaled according to

$$y(\rho, L_{\parallel}, L_{\perp}) = L_{\parallel}^{-\lambda/\nu_{\parallel}} f_{\parallel}[(\rho - \rho_c)L_{\parallel}^{1/\nu_{\parallel}}] \quad (5)$$

$$\equiv L_{\perp}^{-\lambda/\nu_{\perp}} f_{\perp}[(\rho - \rho_c)L_{\perp}^{1/\nu_{\perp}}], \quad (6)$$

where $f_{\parallel}[\cdot]$ and $f_{\perp}[\cdot]$ are unknown scaling functions and λ represents a critical exponent that describes the asymptotic behavior of $y(\rho, L_{\parallel}, L_{\perp})$ in the thermodynamic limit

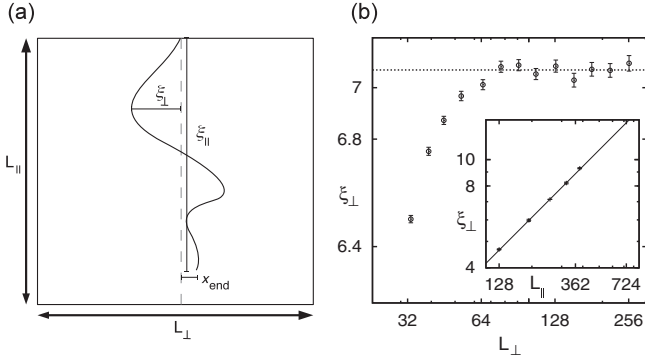


FIG. 5. (a) Sketch of ξ_{\parallel} , ξ_{\perp} , and x_{end} . (b) Correlation length $\xi_{\perp}(L_{\parallel}, L_{\perp})$ as a function of L_{\perp} at $L_{\parallel} = 256$. The inset provides $\theta = 1.59(2)$ (reduced $\chi^2 = 1.7$) according to Eq. (4).

[$y \sim (\rho - \rho_c)^{\lambda}$]. The following is described in regard to Eq. (5) but also apply for Eq. (6) in an analogous manner. Since the scaling function $f_{\parallel}[\cdot]$ does not depend on the system size implicitly, the critical exponents can be found by measuring $y(\rho, L_{\parallel}, L_{\perp})$ for different values of L_{\parallel} (as a consequence L_{\perp} is given, since $L_{\parallel}/L_{\perp}^{\theta}$ is fixed) and ρ in the vicinity of the critical point. If ρ_c , ν_{\parallel} and λ are chosen properly, then all data points of $y(\rho, L_{\parallel}, L_{\perp})L_{\parallel}^{\lambda/\nu_{\parallel}}$ will “collapse” on one single curve by plotting against $(\rho - \rho_c)L_{\parallel}^{1/\nu_{\parallel}}$. The data collapse gives evidence that the correct values of the constants have been found. Note that Eq. (5) shows the scaling behavior for systems that are sufficiently large only [22]. All data collapses in this article are made with a computer-assisted scaling analysis [23].

We have monitored several observables in the vicinity of the expected value of the critical point ($p \in [0.374, 0.395]$). Since we could use fast optimization algorithms, we could study large system sizes in the range $L_{\parallel} = 256$ to $L_{\parallel} = 724$ with good statistics: The data have been obtained by averaging over 30 000 ($L_{\parallel} = 256$), 20 000 ($L_{\parallel} = 362$), 15 000 ($L_{\parallel} = 512$) and 10 000 ($L_{\parallel} = 724$) realizations of the disorder. Figure 6 shows the percolation probability $P_{\text{perc}}(\rho)$ as a

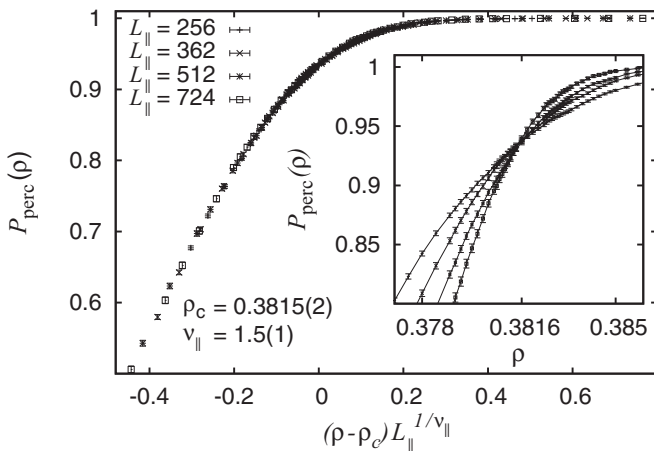


FIG. 6. Percolation probability $P_{\text{perc}}(\rho)$ as a function of ρ in the vicinity of the critical point (inset). The data is collapsed to one curve by using the scaling assumption Eq. (5) (main plot).

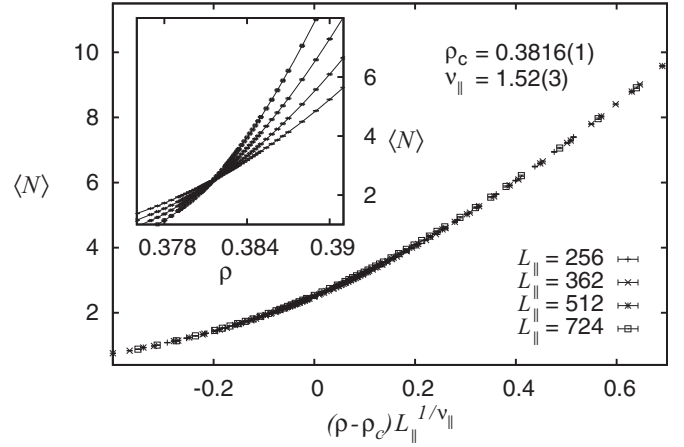


FIG. 7. Average number of spanning loops $\langle N \rangle$ as a function of ρ in the vicinity of the critical point (inset). The data is collapsed to one curve by using the scaling assumption Eq. (5) (main plot).

function of the disorder parameter ρ as well as the rescaled data collapse. Since the percolation probability is constant in both phases [$P_{\text{perc}}(\rho) = 0$ for $\rho < \rho_c$ and $P_{\text{perc}}(\rho) = 1$ for $\rho > \rho_c$], $\lambda = 0$ is set in Eq. (5). The estimates $\rho_c = 0.3815(2)$ and $\nu_{\parallel} = 1.5(1)$ provide the best data collapse with quality $S = 0.7$, which denotes the mean-square distance of the data points to the unknown scaling function in units of the standard error [23]. Using Eq. (6) we have found $\rho_c = 0.3815(2)$ and $\nu_{\perp} = 0.9(2)$. All figures that correspond to Eq. (6) are very similar to their counterparts of Eq. (5) and, therefore, are not shown.

We have also measured the average number of lattice-spanning objects (N); see Fig. 7. Note that, in contrast to standard percolation, more than one object can percolate. By using the data collapse approach, we have found $\rho_c = 0.3816(1)$ and $\nu_{\parallel} = 1.52(3)$ with quality $S = 2.6$. An analysis according to Eq. (6) provides $\rho_c = 0.3816(1)$ and $\nu_{\perp} = 0.95(4)$ with quality $S = 2.7$.

Another quantity that has been under scrutiny is the order parameter

$$P_{\text{node}} = \frac{\langle l \rangle}{L_{\parallel} L_{\perp}}, \quad (7)$$

which is the probability that a bond belongs to either a percolating loop or percolating path. The total number of all bonds that belong to the percolating objects is given by l . The asymptotic behavior of the order parameter is governed by an additional critical exponent β , the percolation strength [24]. For determining β we fixed $\rho_c = 0.3816$, $\nu_{\parallel} = 1.52$ and $\nu_{\perp} = 0.95$, which we have measured before. As evident from Fig. 8, we have found $\beta = 0.95(1)$ with quality $S = 2.4$. A data collapse according to Eq. (6) provides the exact same estimate $\beta = 0.95(1)$ with quality $S = 2.9$.

Next, we consider the associated finite-size susceptibility

$$\chi = \frac{1}{L_{\parallel} L_{\perp}} (\langle l^2 \rangle - \langle l \rangle^2), \quad (8)$$

whose asymptotic behavior is guided by the critical exponent γ . As can be seen from Fig. 9, the best data collapse is provided by $\gamma = 0.54(3)$ with quality $S = 3.2$. Using Eq. (6)

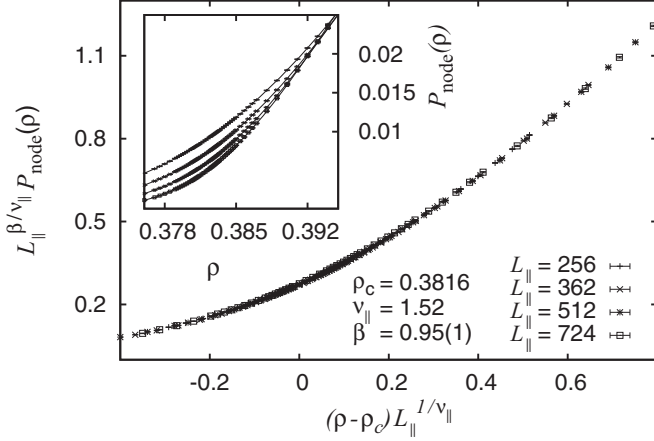


FIG. 8. Order parameter $P_{\text{node}}(\rho)$ as a function of ρ in the vicinity of the critical point (inset). The data is collapsed to one curve by using the scaling assumption Eq. (5) (main plot).

we have found the same estimate $\gamma = 0.54(3)$ with quality $S = 3.5$. Again, $\rho_c = 0.3816$, $v_{\parallel} = 1.52$, and $v_{\perp} = 0.95$ have been fixed.

Right at the critical point, we studied the distribution of path-lengths excluding the lattice-spanning ones. As evident from Fig. 10, the distribution is in good agreement with a power law decay $n_l \sim l^{-\tau}$ with $\tau = 0.750(2)$.

NWP is defined as a global optimization problem (cf. Sec. II) to find the minimally weighted configuration consisting of loops plus one path. Since in the directed polymer problem [13] minimally weighted paths are also selected by global optimization in a random media, these two models might be related. The DPRM can be described as follows: A weighted square lattice, in which all bonds carry a positive weight, gets cut along its diagonal and then it is oriented as a triangle, whose right angle is up. Then all bonds become directed and point either to bottom right or bottom left. On such a lattice, for a given realization of the disorder, one looks for the minimally weighted path that goes from the apex to the base. It has been shown in Ref. [25] that $\zeta^{\circ} = 2/3$, where

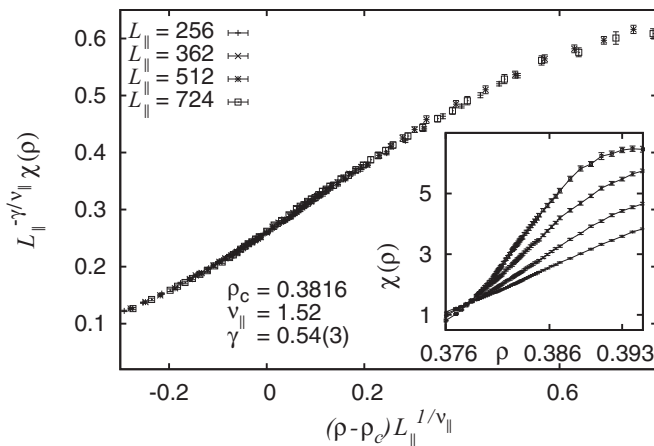


FIG. 9. Fluctuations of the order parameter $\chi_L(\rho)$ over ρ in the vicinity of the critical point (inset). The data is collapsed to one curve by using the scaling assumption Eq. (5) (main plot).

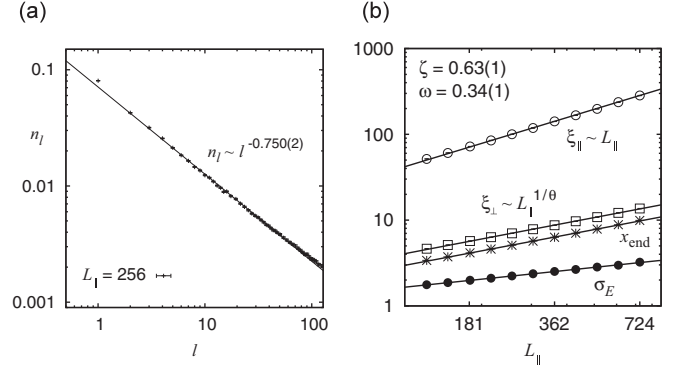


FIG. 10. (a) Distribution of the path lengths l at the critical point excluding those which percolate. 1 000 000 realizations of the disorder have been considered. For the fit (reduced $\chi^2 = 2.4$) path lengths from $l = 2$ to 100 have been taken into account only. (b) Plot shows power-laws as a function of L_{\parallel} for ξ_{\parallel} (linear, reduced $\chi^2 = 2.8$), ξ_{\perp} (exponent $1/\theta$, reduced $\chi^2 = 2.0$), x_{end} (exponent $\zeta = 0.63(1)$, reduced $\chi^2 = 1.8$) and σ_E ($\omega = 0.34(1)$, reduced $\chi^2 = 3.5$). Merely system sizes from $L_{\parallel} = 181$ to 724 have been considered for the power-law regression curves. The measurements are taken at the estimated value of the critical point $\rho_c = 0.3816$.

ζ° is the roughness exponent defined by $D \sim t^{\zeta^{\circ}}$. D describes the mean distance between the base center and the endpoint of the path and t is the size of the triangle, i.e., the length of the path. Furthermore, it is also shown in Ref. [25] that $\omega^{\circ} = 1/3$, which is defined by $\sigma_E \sim t^{\omega^{\circ}}$. σ_E denotes the standard deviation of the weight of the optimal path. A relation between these two exponents is given by the scaling relation $\omega^{\circ} = 2\zeta^{\circ} - 1$ [25]. There are some differences between the optimal path in DPRM and the path that appears in directed NWP. First of all, directed NWP includes the disorder parameter ρ that allows to investigate a percolation transition, which is completely absent for DPRM, since all paths are system spanning by construction. There are also smaller technical differences: For the directed NWP, one looks for an optimal configuration of loops plus one path. The loops, which cannot be crossed by the path, have to be negatively weighted as well and, therefore, block several negatively weighted bonds that cannot be picked up by the path. Thus, this path can not be considered as optimal on its own. Furthermore, while the lengths of the paths in DPRM are always equal, the lengths of the paths in NWP differ considerably.

Nevertheless, in spite of those differences, directed NWP and DPRM might exhibit some scaling which is comparable. To compare both models, we identify $D \leftrightarrow x_{\text{end}}$, where x_{end} is the distance between the endpoint of the path and the line of predominant direction [cf. Fig. 5(a)] and $t \leftrightarrow \xi_{\parallel}$. Since we have monitored the energy values of the paths we can determine also the width σ_E of the energy distribution (which is not important for the percolation transition as studied above). Then we fit for the NWP model to the functions $x_{\text{end}} \sim \xi_{\parallel}^{\zeta}$ and $\sigma_E \sim \xi_{\parallel}^{\omega}$, respectively, while making use of $\xi_{\parallel} \sim L_{\parallel}$ at the critical point. As evident from Fig. 10(b), x_{end} scales with $\zeta = 0.63(1)$ and σ_E with $\omega = 0.34(1)$, which are in reasonably good agreement with the exponents of the DPRM model ($\zeta^{\circ} = 2/3$, $\omega^{\circ} = 1/3$). This agreement is not unnatural, since both models describe some optimal paths in

disordered lattices. Also it shows that the loops which exists in addition to the path in our model, do probably not affect the behavior much, as can be also guessed from the inspection of Fig. 4. Nevertheless, we cannot compare the other exponents we have measured, like β , which describes the typical path lengths, or τ which describes the distribution of path lengths, because these quantities are meaningless for DPRM. Thus, directed NWP exhibits a richer behavior than DPRM although some similarities exist.

IV. SUMMARY AND DISCUSSION

In this work we have studied the directed variant of the negative-weight percolation model. This model defined as a global optimization problem. The model can be studied numerically efficiently, since a mapping to the minimum-weight perfect matching problem exist, such that fast polynomial-time optimization algorithms can be applied. Thus, large systems can be studied numerically with good statistics giving rise to high-quality results. The model exhibits a continuous phase transition, that is characterized by the appearance of loops and a path where at least one of them is large, i.e., system-spanning. We have studied this percolation transition by extended numerical simulations and their analysis based on a finite-size scaling method. By investigating several cluster-related observables we found estimates for the percolation threshold, which we summarized here as $\rho_c = 0.3816(1)$, several critical exponents $\nu_{\parallel} = 1.52(3)$, $\nu_{\perp} = 0.95(4)$, $\beta = 0.95(1)$, $\gamma = 0.54(3)$ and an exponent that describes the power-law decay of the path-length distribution $\tau = 0.750(2)$. For the values of the correlation lengths, we have taken the

estimates which yielded the smallest statistical error bars (from the data collapse of the average number $\langle N \rangle$ of percolating loops). These exponents are in good agreement with the scaling relation $2\beta = \nu_{\parallel} + \nu_{\perp} - \gamma$ [26], where the left and right sides evaluate to 1.90(2) and 1.93(10), respectively. Furthermore, the values we have found show that directed NWP is in a different universality class than standard DP, where [12], e.g., $\nu_{\parallel} = 1.295(6)$, $\nu_{\perp} = 0.733(8)$, $\beta = 0.583(3)$.

Additionally, we have shown that the directed negative-weight percolation model is related to directed polymers in random media (DPRM), although the DPRM does not exhibit a percolation transition (except when diluting the system where just the standard percolation transition appears), thus a less richer behavior than directed NWP.

Clearly, for further studies, it would be interesting to study directed NWP in higher dimensions. Also it could be valuable to verify if the upper critical dimension is four, as for standard directed percolation.

ACKNOWLEDGMENTS

We thank Alfred Hucht for valuable discussions. Financial support was obtained via the Lower Saxony research network ‘‘Smart Nord,’’ which acknowledges the support of the Lower Saxony Ministry of Science and Culture through the ‘‘Niedersächsisches Vorab’’ grant program (Grant No. ZN 2764/ZN 2896). The simulations were performed at the HERO cluster for scientific computing of the University of Oldenburg jointly funded by the DFG (INST 184/108-1 FUGG) and the ministry of Science and Culture (MWK) of the Lower Saxony State.

-
- [1] H. E. Stanley, *Rev. Mod. Phys.* **71**, S358 (1999).
 - [2] D. Stauffer, *Phys. Rep.* **54**, 1 (1979).
 - [3] D. Stauffer and A. Aharony, *Introduction to Percolation Theory* (Taylor & Francis, London, 1992).
 - [4] C. M. Fortuin and P. W. Kasteleyn, *Physica* **57**, 536 (1972).
 - [5] O. Melchert and A. K. Hartmann, *New J. Phys.* **10**, 043039 (2008).
 - [6] L. Apolo, O. Melchert, and A. K. Hartmann, *Phys. Rev. E* **79**, 031103 (2009).
 - [7] O. Melchert, L. Apolo, and A. K. Hartmann, *Phys. Rev. E* **81**, 051108 (2010).
 - [8] O. Melchert and A. K. Hartmann, *Eur. Phys. J. B* **80**, 155 (2011).
 - [9] O. Melchert, A. K. Hartmann, and M. Mézard, *Phys. Rev. E* **84**, 041106 (2011).
 - [10] C. Norrenbrock, O. Melchert, and A. K. Hartmann, *Phys. Rev. E* **87**, 032142 (2013).
 - [11] G. Claussen, L. Apolo, O. Melchert, and A. K. Hartmann, *Phys. Rev. E* **86**, 056708 (2012).
 - [12] H. Hinrichsen, *Adv. Phys.* **49**, 815 (2000).
 - [13] M. Kardar and Y.-C. Zhang, *Phys. Rev. Lett.* **58**, 2087 (1987).
 - [14] A. K. Hartmann, *Big Practical Guide to Computer Simulations* (World Scientific, Singapore, 2015).
 - [15] R. K. Ahuja, T. L. Magnanti, and J. B. Orlin, *Network Flows: Theory, Algorithms, and Applications* (Prentice Hall, New York, 1993).
 - [16] O. Melchert, Ph.D. thesis, Carl-von-Ossietzky Universität, Oldenburg, 2009.
 - [17] W. Cook and A. Rohe, *INFORMS J. Computing* **11**, 138 (1999).
 - [18] A. K. Hartmann and H. Rieger, *Optimization Algorithms in Physics* (Wiley-VCH, Weinheim, 2001).
 - [19] For the calculation of minimum-weighted perfect matchings we use Cook and Rohes blossom4 extension to the Concorde library, URL <http://www2.isye.gatech.edu/~wcook/blossom4/>.
 - [20] S. Angst, A. Hucht, and D. E. Wolf, *Phys. Rev. E* **85**, 051120 (2012).
 - [21] D. Winter, P. Virnau, K. Horbach, and K. Binder, *Europhys. Lett.* **91**, 60002 (2010).
 - [22] K. Binder and D. W. Heermann, *Monte Carlo Simulation in Statistical Physics: An Introduction* (Springer, Berlin, 2002).
 - [23] O. Melchert, [arXiv:0910.5403v1](https://arxiv.org/abs/0910.5403v1).
 - [24] D. Stauffer and A. Aharony, *Introduction to Percolation Theory* (Taylor & Francis, London, 1994).
 - [25] D. A. Huse and C. L. Henley, *Phys. Rev. Lett.* **54**, 2708 (1985).
 - [26] J. W. Essam, A. J. Guttmann, and K. De’Bell, *J. Phys. A* **21**, 3815 (1988).